AN EFFICIENT MULTIGRID CALCULATION OF THE FAR FIELD MAP FOR HELMHOLTZ EQUATIONS

SIEGFRIED COOLS*, BRAM REPS†, AND WIM VANROOSE‡

Abstract. In this paper we present a new highly efficient calculation method for the far field amplitude patterns that arise from scattering problems governed by the d-dimensional Helmholtz equation. The method is based upon a reformulation of the standard real-valued Green's function integral expression for the far field amplitude on a complex contour. On this complex contour the scattered wave can be calculated very efficiently using the iterative multigrid method, resulting in a fast and scalable calculation of the far field mapping. The full complex contour approach is successfully validated on model problems in two and three spatial dimensions.

Key words. Far field map, Helmholtz problem, multigrid method, complex contour.

1. Introduction. Scattering problems are of key importance in many areas of science and engineering since they carry information about an object of interest over large distances, remote from the given target. Consequently, ever since their original statement a variety of applications of scattering problems have arisen in many different scientific subdomains. In chemistry and quantum physics, for example, virtually all knowledge about the inner workings of a molecule has been obtained through scattering experiments [31]. Similarly, in many real-life electromagnetic or acoustic scattering problems information about a far away object is obtained through radar or sonar [15], intrinsically requiring the solution of 2D or 3D wave equation.

Preconditioned Krylov subspace methods are currently among the most efficient numerical algorithms for the solution of high-dimensional equations, as they exploit the sparsity structure of the discretized system of equations and allow for reasonably good scaling with respect to the number of unknowns. Indeed, preconditioned Krylov subspace methods are able to solve some symmetric positive definite systems in only $\mathcal{O}(n)$ iterations, where n is the number of unknowns in the system [44]. However, scattering problem are often described by Helmholtz equations, which after discretization lead to highly indefinite linear systems that are notoriously hard to solve using the current generation of iterative methods. Moreover, the highly efficient iterative multigrid method [9, 11, 12, 42, 43] is known to break down when applied to these type of problems [17, 23].

Over the past decade significant research has been performed on the construction of good preconditioners for Helmholtz problems. Recent work includes the wave-ray approach [10], the idea of separation of variables [33], algebraic multilevel methods [8], multigrid deflation [40] and a transformation of the Helmholtz equation into an advection-diffusion-reaction problem [24]. In 2004 the *Complex Shifted Laplacian (CSL)* preconditioner was proposed by Erlangga, Vuik and Oosterlee [20, 21, 22] as an effective Krylov subspace method preconditioner for Helmholtz problems. The key idea behind this preconditioner is to formulate a perturbed Helmholtz problem that includes a complex valued wave number. Given a sufficiently large complex shift, this implies a damping in the problem, thus making it solvable using multigrid in contrast to the Helmholtz problem with real valued wave numbers. By introducing the complex shifted problem as a preconditioner, the resulting Krylov method has advantageous spectral properties, leading to a reasonable convergence rate. The concept of CSL has been further generalized in a variety of papers among which [2, 18, 19, 32].

Recently a variation on the Complex Shifted Laplacian scheme by the name of *Complex Stretched Grid (CSG)* was proposed in [36, 37], introducing a complex valued grid distance instead of a complex valued wave number in the preconditioning system. It was furthermore shown in [35] that the resulting Krylov subspace method has very similar convergence properties. Indeed, the CSG preconditioner can be shown to be generally equivalent to the CSL scheme, and can thus be solved equally efficiently using multigrid.

The choice of a sufficiently large complex shift parameter, denoted in the literature by β, is vital to the stability of the multigrid solution method. The general rule of the thumb for the choice of

*Dept. Math. & Comp. Sc., University of Antwerp, Middelheimlaan 1, 2020 Antwerp, Belgium
†Dept. Math. & Comp. Sc., University of Antwerp, Middelheimlaan 1, 2020 Antwerp, Belgium
Intel ExaScience Lab, Kapeldreef 75, B-3001 Leuven, Belgium
‡Dept. Math. & Comp. Sc., University of Antwerp, Middelheimlaan 1, 2020 Antwerp, Belgium

the complex shift suggested in the literature is to take $\beta = 0.5$ [21, 35]. This experimental guideline was recently confirmed through a rigorous LFA analysis in [16], proving multigrid to be generally stable for shifts β larger than 0.5.

However, despite its overall qualitative performance the CSL/CSG preconditioned Krylov subspace solution method suffers from a significant wave number dependency of the convergence rate [35]. Additionally, the convergence rate quickly deteriorates in the presence of evanescent waves in the Helmholtz equation.

This paper focuses on calculating the far field mapping resulting from a Helmholtz scattering problem. Typically, the calculation of the far field map is a two step process. First a Helmholtz problem with absorbing boundary conditions is solved on a finite numerical box covering the object of interest. In the second step a volume integral calculates the angular dependency of the far field amplitude with an integral over the Green's function and the numerical solution. This strategy was successfully applied to calculate impact ionization in hydrogen [38] and double photo-ionization in molecules [46, 47] described by the Schrödinger equation, which in this case translates into a 6-dimensional Helmholtz problem.

The absorbing boundary conditions used in this paper are based on the principle of Exterior Complex Scaling (ECS) that was introduced in the 1970's [1, 4, 41] and is frequently used in applications. This method is equivalent to a complex stretching implementation of PML [14].

In this paper we propose a new method for the calculation of the far field map. The method reformulates the integral over the Green's function on a complex contour. This modified approach requires the solution on the Helmholtz equation on a complex contour. It is shown that the latter problem is equivalent to a Complex Shifted Laplacian problem that can be solved very efficiently by using a multigrid method. To validate our approach, the method is successfully illustrated on both 2D and 3D Helmholtz and Schrödinger equations for a variety of discretization levels.

The outline of the article is the following. In Section 2 we briefly define the notation and terminology used throughout the text, and we demonstrate the standard calculation of the far field map for Helmholtz type scattering problems. In the second part of this section we introduce an alternative way of calculating the far field mapping based upon a reformulation of the integral over a complex contour, for which the corresponding Helmholtz system is very efficiently solved iteratively. The new technique is validated on a variety of model scattering problems in both 2D and 3D in Section 3, where it is found to yield a very fast and scalable far field map calculation method. Finally, conclusions are drawn in Section 4.

2. The Helmholtz equation and the far field map. In this section we introduce the general notation used throughout this text and we illustrate the derivation of the far field solution and calculation of its amplitude from a Helmholtz-type scattering problem.

2.1. Derivation of the far field mapping. The Helmholtz equation is a simple mathematical representation of the physics behind a wave scattering at an object defined on a compact support area O located within a domain $\Omega \subset \mathbb{R}^d$. The equation is given by

$$\left(-\Delta - k^2(\boldsymbol{x})\right) u(\boldsymbol{x}) = f(\boldsymbol{x}) \quad \text{on} \quad \Omega \subset \mathbb{R}^d \tag{2.1}$$

with dimension $d \geq 1$, where Δ is the Laplace operator, f designates the right hand side or source term, and k is the (spatially dependent) wave number, representing the material properties inside the object of interest. Indeed, the wave number function k is defined as

$$k(\boldsymbol{x}) = \begin{cases} k(\boldsymbol{x}), & \text{for } \boldsymbol{x} \in O, \\ k_0, & \text{for } \boldsymbol{x} \in \Omega \setminus O, \end{cases} \tag{2.2}$$

where $k_0 \in \mathbb{R}$ is a scalar constant denoting the wave number outside the object of interest. The scattered wave solution is given by the unknown function u. Throughout the text we will use the following convenient notation

$$\chi(\boldsymbol{x}) := \frac{k^2(\boldsymbol{x}) - k_0^2}{k_0^2}, \tag{2.3}$$

such that $k^2(\boldsymbol{x}) = k_0^2\,(1+\chi(\boldsymbol{x}))$. Note that the function χ is trivially zero outside the object of interest O where the space-dependent wave number $k^2(\boldsymbol{x})$ is reduced to k_0. Defining the incoming wave as $u_{in}(\boldsymbol{x}) = e^{ik_0\eta\cdot\boldsymbol{x}}$, where η is the unit vector that defines the direction of the incoming wave, the right-hand side $f(\boldsymbol{x})$ is typically given by $k_0^2\chi(\boldsymbol{x})u_{in}(\boldsymbol{x})$. Reformulating (2.1), we obtain

$$\left(-\Delta - k^2(\boldsymbol{x})\right) u(\boldsymbol{x}) = k_0^2\chi(\boldsymbol{x})u_{in}(\boldsymbol{x}) \qquad \text{for } \boldsymbol{x}\in\Omega. \tag{2.4}$$

This equation is typically formulated on the domain Ω with outgoing wave boundary conditions on $\partial\Omega$. The above equation can in principle be solved in a numerical box (i.e. a discretized subset of Ω) covering the support of χ, with absorbing boundary conditions along all boundaries. Let us assume that the numerical solution satisfying (2.4) on this box has been calculated and is denoted by u^N.

In order to calculate the far field scattered wave pattern the above equation is reorganized as

$$\left(-\Delta - k_0^2\right)\, u(\boldsymbol{x}) = k_0^2\chi(\boldsymbol{x})\left(u_{in}(\boldsymbol{x}) + u(\boldsymbol{x})\right). \tag{2.5}$$

Note that we can replace the function $u(\boldsymbol{x})$ in the right hand side of this equation with the numerical solution $u^N(\boldsymbol{x})$ obtained from equation (2.4). In doing so, the above equation becomes an inhomogeneous Helmholtz equation with constant wave number

$$\left(-\Delta - k_0^2\right)\, u(\boldsymbol{x}) = g(\boldsymbol{x}) \quad \text{for } \boldsymbol{x}\in\mathbb{R}^d, \tag{2.6}$$

where the short notation $g(\boldsymbol{x}) = k_0^2\chi(\boldsymbol{x})(u_{in}(\boldsymbol{x})+u^N(\boldsymbol{x}))$ is introduced for readability and notational convenience. The above equation can easily be solved analytically using Green's function $G(\boldsymbol{x},\boldsymbol{x}')$, i.e.

$$u(\boldsymbol{x}) = \int_{\mathbb{R}^d} G(\boldsymbol{x},\boldsymbol{x}')\, g(\boldsymbol{x}')\, d\boldsymbol{x}'. \tag{2.7}$$

Since the function g is only non-zero inside the numerical box that was used to solve equation (2.4), the above integral over $\mathbb{R}^d$ can be replaced by a finite integral over Ω

$$u(\boldsymbol{x}) = \int_{\Omega} G(\boldsymbol{x},\boldsymbol{x}')k_0^2\chi(\boldsymbol{x}')\left(u_{in}(\boldsymbol{x}') + u^N(\boldsymbol{x}')\right)\, d\boldsymbol{x}' \qquad \text{for } \boldsymbol{x}\in\mathbb{R}^d. \tag{2.8}$$

This expression allows us to calculate the scattered wave solution u in any point $\boldsymbol{x}\in\mathbb{R}^d$ *outside* the numerical box, using only the information *inside* the numerical box.

Given the integral expression (2.8), the asymptotic form of the Green's function can be used to compute the far field mapping of the scattered wave u. In the following this will be illustrated for a 2D model example where the Green's function is given explicitly by

$$G(\boldsymbol{x},\boldsymbol{x}') = \frac{i}{4}H_0^{(1)}(k_0|\boldsymbol{x}-\boldsymbol{x}'|), \tag{2.9}$$

where i represents the imaginary unit and $H_0^{(1)}$ is the 0-th order Hankel function of the first kind. Note that an analogous derivation can be performed in 3D, where we mention for completeness that the Green's function is given by

$$G(\boldsymbol{x},\boldsymbol{x}') = \frac{e^{ik_0|\boldsymbol{x}-\boldsymbol{x}'|}}{4\pi|\boldsymbol{x}-\boldsymbol{x}'|}. \tag{2.10}$$

To calculate the angular dependence of the far field map, the direction of the unit vector $\boldsymbol{\alpha}$ is introduced that is in 2D defined by a single angle α with the positive horizontal axis, i.e. $\boldsymbol{\alpha} = (\cos\alpha, \sin\alpha)^T$. Rewriting the spatial coordinates $\boldsymbol{x}$ in polar coordinates as $\boldsymbol{x} = (\rho\cos\alpha, \rho\sin\alpha)^T$ the asymptotic form of the Green's function for $|\boldsymbol{x}| \gg 1$ ($\rho\to\infty$) is given by

$$\begin{aligned}\frac{i}{4}H_0^{(1)}(k_0|\boldsymbol{x}-\boldsymbol{x}'|) &= \frac{i}{4}\sqrt{\frac{2}{\pi}}e^{-i\pi/4}\frac{1}{\sqrt{k_0\rho}}e^{ik_0\rho}e^{-ik_0x'\cos\alpha - ik_0y'\sin\alpha} \\ &= \frac{i}{4}\sqrt{\frac{2}{\pi}}e^{-i\pi/4}\frac{1}{\sqrt{k_0\rho}}e^{ik_0\rho}e^{-ik_0\boldsymbol{x}'\cdot\boldsymbol{\alpha}}\end{aligned} \tag{2.11}$$

where we have used the fact that the Hankel function $H_0^{(1)}$ is asymptotically given by

$$H_0^{(1)}(r) = \sqrt{\frac{2}{\pi r}} \exp\left(i(r - \frac{\pi}{4})\right), \qquad r \in \mathbb{R}, \quad r \gg 1. \tag{2.12}$$

This leads to the following asymptotic form of the 2D scattered wave solution

$$u(\rho, \alpha) = \frac{i}{4}\sqrt{\frac{2}{\pi}} e^{-i\pi/4} \frac{e^{ik_0\rho}}{\sqrt{k_0\rho}} \int_\Omega e^{-ik_0 \boldsymbol{x}'\cdot\boldsymbol{\alpha}} g(\boldsymbol{x}')\, d\boldsymbol{x}', \tag{2.13}$$

for $\rho \to \infty$. The above expression is called the 2D *far field wave pattern* of u, with the integral being denoted as the *far field (amplitude) map*

$$F(\boldsymbol{\alpha}) = \int_\Omega e^{-ik_0 \boldsymbol{x}'\cdot\boldsymbol{\alpha}} g(\boldsymbol{x}')\, d\boldsymbol{x}'. \tag{2.14}$$

Note that the value of the integral only depends on the direction $\boldsymbol{\alpha}$ (or, in 2D, on the angle α) and the wave number k_0. Expression (2.13) readily extends to the d-dimensional case, where it holds more generally that

$$\lim_{\rho\to\infty} u(\rho, \boldsymbol{\alpha}) = D(\rho)F(\boldsymbol{\alpha}), \qquad \boldsymbol{\alpha} \in \mathbb{R}^d, \tag{2.15}$$

for a function $D(\rho)$ which is known explicitly and a far field mapping $F(\boldsymbol{\alpha})$ given by (2.14). This far field mapping is in fact a Fourier integral of the function g.

Summarizing, we conclude that the calculation of the far field wave pattern of the scattered wave u consists of two main steps. First, one has to solve a Helmholtz equation with a spatially dependent wave number on a numerical box with absorbing boundary conditions as in (2.4). Once the numerical solution is obtained, it is followed by the calculation of a Fourier integral (2.14) over the aforementioned numerical domain. The main computational bottleneck of this calculation generally lies within the first step, since one requires a suitable (iterative) method for the solution of a high dimensional indefinite Helmholtz system with absorbing boundary conditions.

Note that the statement of the far field mapping presented in this section relies on the fact that the object of interest function χ is compactly supported. In particular, this is used when computing the numerical solution u^N to equation (2.4) on a bounded numerical box that covers the support of χ. The above reasoning can however be readily extended to the more general class of analytical object functions χ that vanish at infinity, i.e. $\chi \in V$ where $V = \{f : \mathbb{R}^d \to \mathbb{R} \text{ analytical} \mid \forall \varepsilon > 0, \exists K \subset \mathbb{R}^d \text{ compact}, \forall x \in \mathbb{R}^d \setminus K : |f(x)| < \varepsilon\}$. Indeed, due to the existence of smooth bump functions [27, 30], functions with compact support can be shown to be dense within the space of functions that vanish at infinity. Consequently, every analytical function χ that vanishes at infinity can be arbitrarily closely approximated by a series of compactly supported functions $\{\chi_n\}_n$. This in turn implies that the corresponding solutions $\{u_n^N\}_n$ on a limited computational box can be arbitrarily close to the solution of the Helmholtz equation generated with the analytical object of interest $\chi \in V$. Intuitively, this means that if χ is analytical but sufficiently small everywhere outside O, the computational domain may be retricted to a numerical box covering O as though χ was compactly supported. Hence, the far field mapping (2.14) is well-defined for analytical functions χ that vanish at infinity. This observation will prove particularly useful in the next section.

2.2. Calculation on a complex contour. In this paragraph we will illustrate how the integral (2.14) can be reformulated on a complex contour and why this is useful in terms of numerical computation. First, we note that the integral can be split into a sum of two contributions $F(\boldsymbol{\alpha}) = I_1 + I_2$ with

$$I_1 = \int_\Omega e^{-ik_0\boldsymbol{x}\cdot\boldsymbol{\alpha}} \chi(\boldsymbol{x}) u_{in}(\boldsymbol{x}) d\boldsymbol{x} \quad \text{and} \quad I_2 = \int_\Omega e^{-ik_0\boldsymbol{x}\cdot\boldsymbol{\alpha}} \chi(\boldsymbol{x}) u^N(\boldsymbol{x}) d\boldsymbol{x}. \tag{2.16}$$

Calculation of first integral I_1 is generally easy, since it only requires the expression for the incoming wave, which is known analytically. The second integral however requires the solution of the Helmholtz

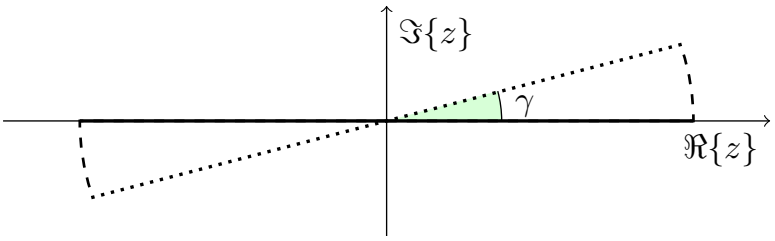

FIG. 2.1. *Schematic representation of the complex contour for the far field integral calculation illustrated in 1D. The full line represents the real domain Ω, the dotted and dashed lines represent the subareas $Z_1 = \{\boldsymbol{x}e^{i\gamma} : \boldsymbol{x} \in \Omega\}$ and $Z_2 = \{\boldsymbol{b}e^{i\theta} : \boldsymbol{b} \in \partial\Omega,\ \theta \in [0, \gamma]\}$ of the complex contour respectively.*

equation on the numerical box, which is known to be notoriously hard to obtain using iterative methods. In particular, the highly efficient multigrid solution method is unable to solve these type of indefinite Helmholtz equations due to instability in both the coarse grid correction and relaxation scheme. This divergence is due to close-to-zero eigenvalues of the discretized operator on some intermediate multigrid levels [17].

However, if both u and χ are analytical functions the integral can be calculated over a complex contour rather than the real axis as follows. Let us define a complex contour along the rotated real domain $Z_1 = \{\boldsymbol{z} \in \mathbb{C} \,|\, \boldsymbol{z} = \boldsymbol{x}e^{i\gamma} : \boldsymbol{x} \in \Omega\}$, where γ is a fixed rotation angle, followed by the curved segment $Z_2 = \{\boldsymbol{z} \in \mathbb{C} \,|\, \boldsymbol{z} = \boldsymbol{b}e^{i\theta} : \boldsymbol{b} \in \partial\Omega,\ 0 \leq \theta \leq \gamma\}$, as presented schematically on Figure 2.1. The integral I_2 can then be written as

$$I_2 = \int_{Z_1} e^{-ik_0 \boldsymbol{z}\cdot\boldsymbol{\alpha}} \chi(\boldsymbol{z}) u^N(\boldsymbol{z}) d\boldsymbol{z} + \int_{Z_2} e^{-ik_0 \boldsymbol{z}\cdot\boldsymbol{\alpha}} \chi(\boldsymbol{z}) u^N(\boldsymbol{z}) d\boldsymbol{z}. \tag{2.17}$$

The second term in the above expression however vanishes, as the function χ is per definition zero everywhere outside the object of interest O, thus notably in all points $\boldsymbol{z} \in Z_2$. Hence one ultimately obtains

$$I_2 = \int_{Z_1} e^{-ik_0 \boldsymbol{z}\cdot\boldsymbol{\alpha}} \chi(\boldsymbol{z}) u^N(\boldsymbol{z}) d\boldsymbol{z} = \int_{\Omega} e^{-ik_0 e^{i\gamma}\boldsymbol{x}\cdot\boldsymbol{\alpha}} \chi(\boldsymbol{x}e^{i\gamma}) u^N(\boldsymbol{x}e^{i\gamma}) e^{i\gamma}\, d\boldsymbol{x}. \tag{2.18}$$

Note that for $0 < \gamma < \pi/2$ the exponential of $\boldsymbol{x}e^{i\gamma}$ is increasing in all directions. At the same time the scattered wave solution u^N, which consists of outgoing waves on the complex domain Z_1, is decaying in all directions. Additionally, the function χ is presumed to have a bounded support making the above integral calculable on a limited numerical domain.

Expression (2.18) for the integral I_2 indicates that the far field map can (at least partially) be computed over the full complex contour Z_1, i.e. a rotation of the original real domain Ω over an angle γ in all spatial dimensions. The advantage of this approach is that we only need the value of u^N evaluated along this complex contour; thus we now have to solve the Helmholtz equation (2.4) on a complex contour. On this contour it is a damped equation which is much easier to solve that the Helmholtz equation along the real axis. Indeed, given a sufficiently large value of γ, it has been shown in the literature [22, 36] that the multigrid scheme is a very effective solution method for the Helmholtz equation on a complex domain.

2.3. Solving the Helmholtz equation on a complex contour. We now show that the Helmholtz problem on the complex domain Z_1 is similar to a complex shifted Laplacian system [20], and can thus be solved very efficiently using a multigrid solver. Consider the Helmholtz problem with a complex shifted wave number

$$\left(-\Delta - (1 + i\beta)k^2(\boldsymbol{x})\right) u(\boldsymbol{x}) = f(\boldsymbol{x}) \tag{2.19}$$

with Dirichlet boundary conditions $u(\boldsymbol{x}|_{\partial\Omega}) = 0$ and a complex shift parameter $\beta \in \mathbb{R}$. After finite difference discretization on a d-dimensional Cartesian grid with fixed grid distance h in every spatial

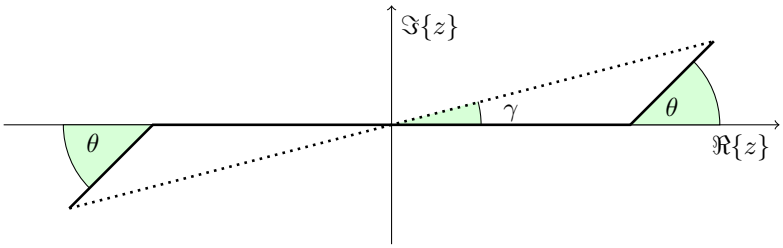

FIG. 2.2. *Real grid with ECS boundaries vs. full complex grid.*

dimension, one typically obtains a linear system

$$-\left(\frac{1}{h^2}L + (1+i\beta)k^2\right)u_h = b_h \tag{2.20}$$

where L is the matrix operator expressing the stencil structure of the Laplacian. In 2D, for example $L = \text{kron}(I, \text{diag}(-1, 2, -1) + \text{kron}(\text{diag}(-1, 2, -1), I)$, where the size of L intrinsically depends on h. After dividing both sides in linear system (2.20) by $(1+i\beta)$, we immediately obtain the equivalent system

$$-\left(\frac{1}{(1+i\beta)h^2}L + k^2\right)u_h = \frac{b_h}{1+i\beta}, \tag{2.21}$$

which is identical to the discretization of the original Laplacian with grid distance $\tilde{h} = \sqrt{1+i\beta}\,h$. This scheme is known as *Complex Stretched Grid*, and it was shown in [36] to yield exactly the same Krylov convergence compared to Complex Shifted Laplacian when both are used as a preconditioner for a general Krylov method.

It is known from the literature [16, 20] that problem (2.20), or equivalently (2.21), can be solved efficiently with multigrid for values of the complex shift $\beta > 0.5$. Note that this requirement is based on a multigrid cycle with standard weighted Jacobi or Gauss-Seidel smoothing. This rule of thumb can easily be translated into an angle γ for the complex scaling. Writing $(1+i\beta) = \rho\exp(i\varphi)$ with $\rho = \sqrt{1+\beta^2}$ and $\varphi = \arctan\beta$, one readily obtains

$$\tilde{h} = \sqrt{1+i\beta}\,h = \sqrt{\rho}\exp(i\varphi/2)h \tag{2.22}$$

Consequently, as the shift β is required to be larger than 0.5, the grid rotation angle $\gamma = \varphi/2$ must satisfy

$$\gamma > \frac{\arctan(0.5)}{2} = 0.2318 \approx 13.28^\circ \tag{2.23}$$

Note that when substituting the standard multigrid relaxation schemes like ω-Jacobi or Gauss-Seidel by a more robust iterative scheme like e.g. GMRES(m), the rotation angle γ may be chosen even smaller, up to a minimum of approximately 9.5° (see [34]).

In this paper we have chosen to link the grid rotation angle γ to the standard ECS absorbing layer angle θ, see Figure 2.2. This is in no way imperious for the functionality of the method, but it appears quite naturally from the fact that both angles perturb (part of) the grid into the complex plane. Suppose the ECS boundary layer measures one quarter of the length of the entire real domain in every spatial dimension, which is a common choice, we readily derive that the relation between the rotation angle γ and the ECS angle θ is given by

$$\gamma = \arctan\left(\frac{\sin\theta}{2+\cos\theta}\right). \tag{2.24}$$

Table 2.1 shows some standard values of the ECS angle θ and corresponding γ values according to (2.24). Note that for a multigrid scheme with ω-Jacobi or Gauss-Seidel smoothing to be stable, θ should be chosen no smaller than $\pi/4$, see (2.23). Using the more efficient GMRES(3) method as a smoother, the ECS angle can be chosen somewhat smaller, i.e. an angle around $\theta = \pi/6$ suffices to guarantee a stable multigrid solution.

θ (rad.)	$\pi/8$	$\pi/6$	$\pi/5$	$\pi/4$	$\pi/3$
γ (deg.)	7.5°	9.9°	11.8°	14.6°	19.1°

TABLE 2.1
ECS angle θ and corresponding rotation angle γ for the full complex grid. Values based on (2.24).

3. Numerical results for 2D and 3D Helmholtz problems. In this section, we validate the theoretical result presented above by a number of numerical experiments in both two and three spatial dimensions. It will be shown that the proposed method results in a very fast and wave number-independent solution method for the scattered wave system, hence yielding a remarkably efficient method for the calculation of the far field mapping.

The model problem used throughout this section is a Helmholtz equation of the form (2.4) with $k^2(\boldsymbol{x}) = k_0^2(1 + \chi(\boldsymbol{x}))$. The equation is discretized on a n^d-point uniform mesh covering a square numerical domain $\Omega = [-20, 20]^d$ using second order finite differences. In the 2D case the space-dependent wave number is defined as

$$\chi(x, y) = -1/5 \left(e^{-(x^2+(y-4)^2)} + e^{-(x^2+(y+4)^2)} \right), \quad (x, y) \in [-20, 20]^2, \tag{3.1}$$

i.e. the object of interest takes the form of two circular point-like objects with mass concentrated at the Cartesian coordinates $(0, -4)$ and $(0, 4)$ (see Figure 3.1). For the 3D model problem, the following straightforward extension of the object is used

$$\chi(x, y, z) = -1/5 \left(e^{-(x^2+(y-4)^2+z^2)} + e^{-(x^2+(y+4)^2+z^2)} \right), \quad (x, y, z) \in [-20, 20]^3, \tag{3.2}$$

representing two spherical point-like objects in 3D space (see Figure 3.2). The incoming wave scattering at the given object is defined by

$$u_{in}(\boldsymbol{x}) = e^{ik_0 \boldsymbol{\eta} \cdot \boldsymbol{x}}, \quad \boldsymbol{x} \in \Omega, \tag{3.3}$$

where $\boldsymbol{\eta}$ is the unit vector in the x-direction.

Figure 3.1 illustrates the theoretical result presented in Section 2. The above 2D Helmholtz model problem with wave number given by (3.1) is solved for u^N using respectively a standard LU factorization method on the real domain Ω with ECS complex boundary layers ($\theta = \pi/4$) along the domain boundary $\partial\Omega$, and a series of multigrid V(1,1)-cycles with ω-Jacobi smoothing on the full complex domain ($\gamma \approx 14.6°$) up to residual tolerance `1e-6`. The standard multigrid intergrid operators used in this work are bilinear interpolation and full weighting restriction. The moduli of the wave number function χ (top) and the resulting solution u^N (mid) are shown on Figure 3.1 for both methods. Note how the solution u^N on the full complex contour is indeed heavily damped compared to the solution on the real domain. Consequently, using the numerical solution u^N, the 2D far field map integral (2.14) can be calculated using any numerical integration scheme over the real or complex domain respectively. The resulting far field mapping $F(\boldsymbol{\alpha})$ is shown as a function of the angle α on Figure 3.1 (bottom). One observes that the mapping is indeed identical when calculated on the real and complex domain, conform with the theoretical results. However, the computational cost of the real-domain method for calculation of the far field map is reduced significantly by the ability to apply multigrid to the equivalent complex scaled problem.

In Table 3.1 convergence results are shown for the solution of the 3D scattered wave equation (2.4) using a series of multigrid V(1,1)-cycles on various grid sizes. Note that the multigrid method scales perfectly as a function of the number of grid points, as doubling the number of grid points in every spatial dimension does not increase the number of V-cycles required to reach a fixed residual tolerance of `1e-6`. This is a standard result from multigrid theory. Additionally and more importantly, remarkable k-scalability is measured for the multigrid solution method on the complex contour. Indeed, the multigrid convergence factor (and thus the corresponding work unit load required to solve the problem up to a given tolerance) is almost fully independent of the wave number k_0, as can be observed from the table. Note that from a physical-numerical point of view it is only

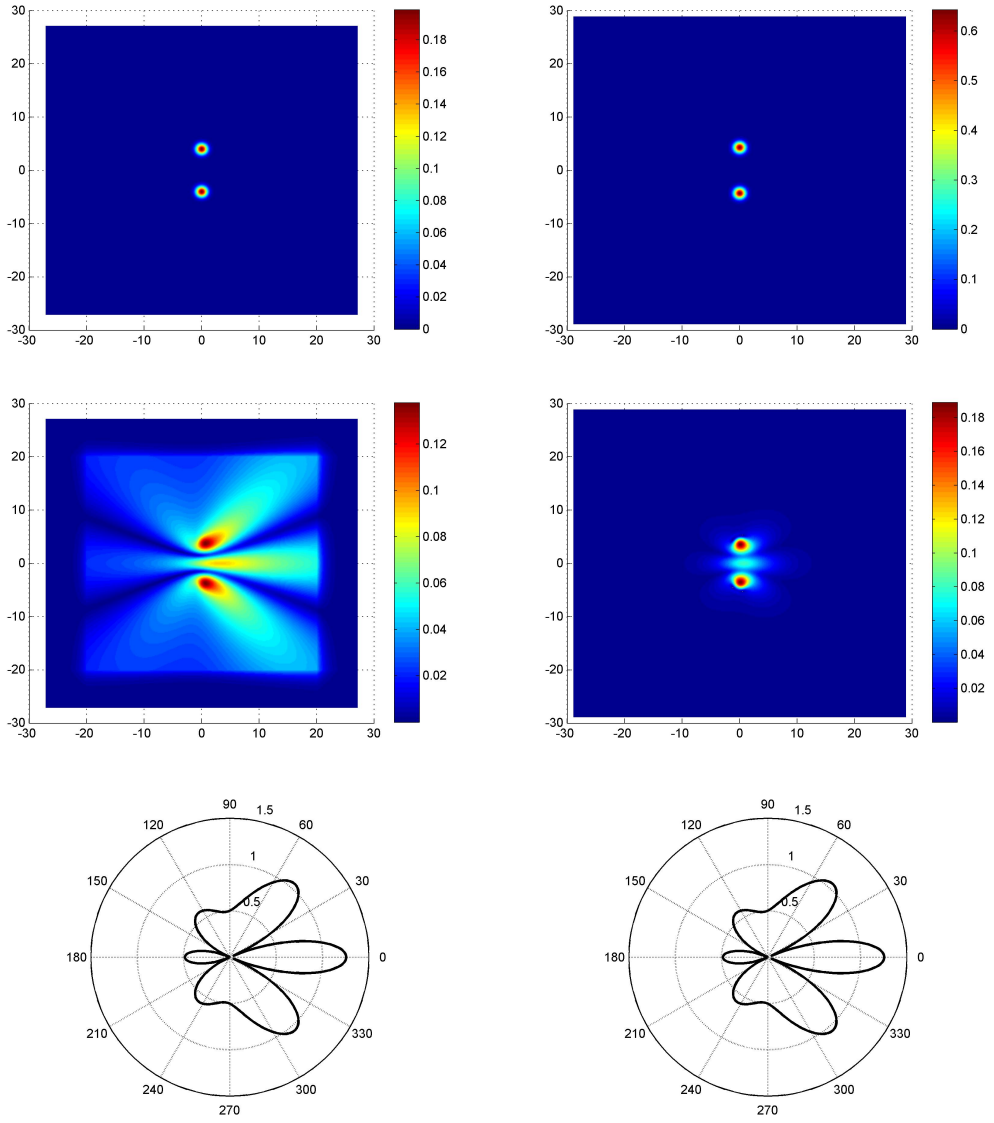

FIG. 3.1. *Top: 2D object of interest* $|\chi(\boldsymbol{x})|$ *given by (3.1). Mid: solution to the Helmholtz problem (2.4) (in modulus) on a* $n_x \times n_y = 256 \times 256$ *grid solved using LU factorization (left) on a double ECS contour with* $\theta = \pi/4$*, and using a series of multigrid V-cycles (right) with* ω*-Jacobi smoother on the corresponding full complex contour up to a residual reduction tolerance of* `1e-6`*. Bottom: resulting 2D Far field maps* $F(\alpha)$ *calculated following (2.14).*

meaningful to consider discretizations satisfying the $k_0 h < 0.625$ criterion for a minimum of 10 grid points per wavelength, cfr. [6], for which the corresponding values are designated in Table 3.1 by a bold typesetting.

Ultimately, the computed scattered wave solution on the complex domain can again be used to calculate the far field integral (2.14). The resulting 3D far field mapping for the model problem with $k_0 = 1$ is plotted in Figure 3.2. The left hand side panel shows an iso-surface visualization of the 3D object of interest $\chi(\boldsymbol{x})$ given by (3.2). On the right panel a spherical projection of the resulting 3D far field mapping is shown. The color hue indicates the value of the far field amplitude in each outgoing direction.

Note that the calculation of the scattered wave solution can be optimized even further by considering the *Full Multigrid (FMG)* scheme. This is a nested iteration of standard V-cycles, where on each level a series of V(1,1)-cycles is used to approximately solve the error equation and supply

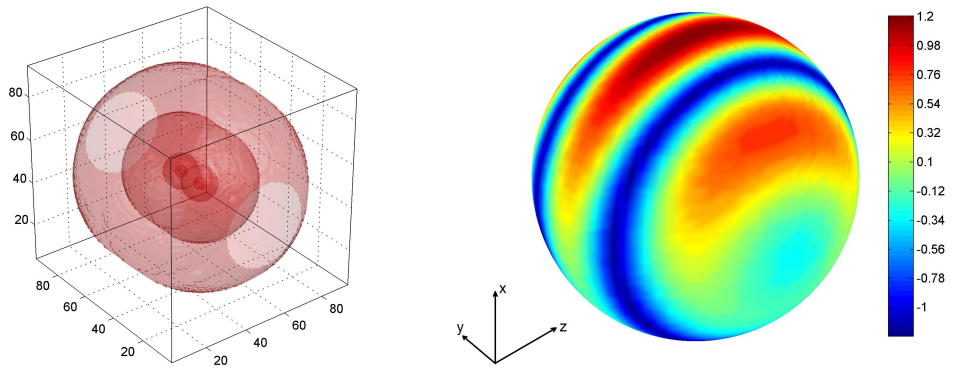

FIG. 3.2. *Left: 3D object of interest $|\chi(\boldsymbol{x})|$ given by (3.2). Shown are the $|\chi(\boldsymbol{x})| = c$ isosurfaces for $c =$ 0, `1e-2`, `1e-10` and `1e-100`. Right: 3D Far field map, resulting from Helmholtz problem (2.4) with $k_0 = 1$ solved on a $n_x \times n_y \times n_z = 64 \times 64 \times 64$ full complex grid with $\theta = \pi/6$ ($\gamma \approx 9.9°$) using a series of multigrid V-cycles with GMRES(3) smoother up to residual reduction tolerance `1e-6`.*

	$n_x \times n_y \times n_z$	16^3	32^3	64^3	128^3	256^3
k_0	1/4	**10** (10) 0.24	**9** (59) 0.20	**9** (560) 0.21	**9** (4456) 0.20	**9** (35165) 0.20
	1/2	12 (12) 0.31	**10** (63) 0.24	**10** (611) 0.22	**10** (4937) 0.23	**9** (35405) 0.21
	1	7 (8) 0.13	13 (83) 0.32	**11** (691) 0.27	**10** (4899) 0.24	**10** (38975) 0.24
	2	2 (4) 0.01	8 (54) 0.14	13 (809) 0.33	**11** (5418) 0.27	**10** (38051) 0.24
	4	1 (3) 0.01	2 (17) 0.01	7 (457) 0.12	13 (6337) 0.33	**11** (41848) 0.26

TABLE 3.1

3D Helmholtz problem (2.4) solved on a full complex grid with $\theta = \pi/6$ using a series of multigrid V(1,1)-cycles with GMRES(3) smoother up to residual reduction tolerance `1e-6`. Displayed are the number of V-cycle iterations, number of work units and average convergence factor for various wave numbers k_0 and different discretizations. 1 WU is calibrated as the cost of 1 V(1,1)-cycle on the 16^3-points grid $k_0 = 1/4$ problem. Discretizations respecting the $k_0 h < 0.625$ criterion for a minimum of 10 grid points per wavelength are indicated by a bold typesetting.

a corrected initial guess for a finer level by interpolating the corresponding coarse grid solution.

Table 3.2 shows convergence results for the solution of the 3D scattered wave equation (2.4) using an FMG scheme. The setting is comparable to that of Table 3.1, as a residual reduction tolerance of 10^{-6} is imposed for each wavenumber and at every level of the FMG cycle, yielding a fine $n_x \times n_y \times n_z = 256^3$ grid residual of order of magnitude 10^{-9}. Note that the number of V-cycles performed on each level in the FMG cycle is decaying in function of the growing grid size due to the increasingly accurate initial guess, resulting in a relatively small number of V-cycles (**5-9**) to be performed on the finest level. Consequently, the number of work units (and thus the computational time) required to reach the designated residual reduction tolerance is significantly lower than the work unit load of the pure V-cycle scheme displayed in Table 3.1.

Timing and residual results from a standard FMG sweep performing only one V(1,1)-cycle on each level on the 3D Helmholtz scattering problem with a moderate wave number $k_0 = 1$ are shown in Table 3.3 for different discretizations. Note that timings were generated using a basic non-parallelised Matlab code, using only a single thread on a simple midrange personal computer and taking less than 8 minutes to solve a 3D Helmholtz problem with 256 gridpoints in every spatial dimension.

	$n_x \times n_y \times n_z$	16^3	32^3	64^3	128^3	256^3
k_0	1/4	**8** (11) 1.93e-9	**6** (52) 1.77e-9	**5** (384) 2.46e-9	**5** (3190) 2.68e-9	**5** (25241) 3.00e-9
	1/2	9 (12) 1.27e-8	**8** (68) 1.87e-9	**6** (452) 3.37e-9	**6** (3392) 1.30e-9	**6** (30215) 1.25e-9
	1	5 (8) 1.33e-8	9 (68) 1.51e-8	**8** (572) 4.07e-9	**7** (4013) 1.76e-9	**6** (30747) 3.66e-9
	2	1 (5) 5.99e-13	5 (43) 1.18e-8	9 (600) 1.91e-8	**8** (4456) 5.28e-9	**7** (36367) 2.67e-9
	4	1 (4) 8.90e-20	1 (18) 2.86e-13	5 (357) 5.19e-9	9 (5038) 1.97e-8	**8** (39038) 4.65e-9

TABLE 3.2

3D Helmholtz problem (2.4) solved on a full complex grid with $\theta = \pi/6$ using an FMG cycle with GMRES(3) smoother up to residual reduction tolerance of `1e-6`. Displayed are the number of V-cycle iterations on the designated finest grid, number of work units and resulting residual norm for various wave numbers k_0 and different discretizations. 1 WU is calibrated as the cost of 1 V(1,1)-cycle on the 16^3-points grid $k_0 = 1/4$ problem. Discretizations respecting the $k_0 h < 0.625$ criterion for a minimum of 10 grid points per wavelength indicated by a bold typesetting.

$n_x \times n_y \times n_z$	16^3	32^3	64^3	128^3	256^3
CPU time	0.20 s.	0.78 s.	6.24 s.	53.3 s.	462 s.
$\|r\|_2$	3.3e-5	7.9e-5	2.7e-5	1.1e-5	4.6e-6

TABLE 3.3

3D Helmholtz problem (2.4) with wave number $k_0 = 1$ solved on a full complex grid with $\theta = \pi/6$ using one FMG-cycle with GMRES(3) smoother. Displayed are the CPU time (in s.) and the resulting residual norm for various discretizations. System specifications: Intel® Core™ i7-2720QM 2.20GHz CPU, 6MB Cache, 8GB RAM.

4. Conclusions and discussion. In this paper we have developed a novel highly efficient method for the calculation of the far field map resulting from d-dimensional Helmholtz scattering problems where the wave number is an analytical function. Our approach is based on the reformulation of the classically real-valued Green's function volume integral for the far field map to an equivalent volume integral over a complex valued domain.

The advantage of the proposed reformulation lies in the scattered wave solution of the Helmholtz problem on a complex domain, which for high dimensional problems can be calculated efficiently using a multigrid method. Indeed, the reformulation of the Helmholtz forward problem on the full complex contour is shown to be equivalent to a Complex Shifted Laplacian problem, where multigrid has been proven in the literature to be a fast and scalable solver. However, whereas the Complex Shifted Laplacian was previously only used as a preconditioner for highly indefinite Helmholtz problems, the complex-valued far field map calculation proposed within this paper effectively allows for multigrid to be used as a solver.

The functionality of the method is validated on 2D and 3D model Helmholtz problems. It is confirmed that the values of the far field mapping calculated on the full complex grid exactly matches the values of the classical real-valued integral. Furthermore, the number of multigrid iterations is shown to be largely wave number independent, yielding a fast overall far field map calculation.

One area of scientific computing where the proposed technique might be particularly valuable is in the numerical solution of quantum mechanical scattering problems. These are generally high-dimensional scattering problems where the wave number is indeed an analytical function and where 6D or 9D problems are common.

Finally we note that a number of modifications can be made to improve the efficiency of the method even further, e.g. choosing the complex contour for the integral based on a steepest descent scheme as proposed in [26].

5. Acknowledgments. This research was partly funded by the *Fonds voor Wetenschappelijk Onderzoek (FWO)* project G.0.120.08 and *Krediet aan navorser* project number 1.5.145.10. Additionally, this work was partly funded by Intel® and by the *Institute for the Promotion of Innovation through Science and Technology in Flanders (IWT)*. The authors would like to thank Hisham bin Zubair for sharing a multigrid implementation and Daan Huybrechs for fruitful discussions on the subject.

REFERENCES

[1] J. Aguilar and J.M. Combes. A class of analytic perturbations for one-body Schrödinger Hamiltonians. *Communications in Mathematical Physics*, 22(4):269–279, 1971.

[2] T. Airaksinen, E. Heikkola, A. Pennanen, and J. Toivanen. An algebraic multigrid based shifted-Laplacian preconditioner for the Helmholtz equation. *Journal of Computational Physics*, 226(1):1196–1210, 2009.

[3] M. Baertschy, T.N. Rescigno, W.A. Isaacs, X. Li, and C.W. McCurdy. Electron-impact ionization of atomic hydrogen. *Physical Review A*, 63(2):022712, 2001.

[4] E. Balslev and J.M. Combes. Spectral properties of many-body schrödinger operators with dilatation-analytic interactions. *Communications in Mathematical Physics*, 22(4):280–294, 1971.

[5] A. Bayliss, C.I. Goldstein, and E. Turkel. An iterative method for the helmholtz equation. *Journal of Computational Physics*, 49(3):443–457, 1983.

[6] A. Bayliss, C.I. Goldstein, and E. Turkel. On accuracy conditions for the numerical computation of waves. *Journal of Computational Physics*, 59(3):396–404, 1985.

[7] H. bin Zubair, B. Reps, and W. Vanroose. A preconditioned iterative solver for the scattering solutions of the schrödinger equation. *Communications in Computational Physics*, 11(2):415, 2012.

[8] M. Bollhöfer, M.J. Grote, and O. Schenk. Algebraic multilevel preconditioner for the Helmholtz equation in heterogeneous media. *SIAM Journal on Scientific Computing*, 31(5):3781–3805, 2009.

[9] A. Brandt. Multi-level adaptive solutions to boundary-value problems. *Mathematics of computation*, 31(138):333–390, 1977.

[10] A. Brandt and I. Livshits. Wave-ray multigrid method for standing wave equations. *Electronic Transactions on Numerical Analysis*, 6:162–181, 1997.

[11] A. Brandt and S. Ta'asan. Multigrid method for nearly singular and slightly indefinite problems. *Multigrid Methods II, Lecture Notes in Math.*, 1228:99–121, 1986.

[12] W.L. Briggs, V.E. Henson, and S.F. McCormick. *A multigrid tutorial*. Society for Industrial Mathematics, Philadelphia, 2000.

[13] H. Calandra, S. Gratton, R. Lago, X. Pinel, and X. Vasseur. Two-level preconditioned Krylov subspace methods for the solution of three-dimensional heterogeneous Helmholtz problems in seismics. Technical report, TR/PA/11/80, CERFACS, Toulouse, France, 2011.3, 2011.

[14] W.C. Chew and W.H. Weedon. A 3d perfectly matched medium from modified maxwell's equations with stretched coordinates. *Microwave and optical technology letters*, 7(13):599–604, 2007.

[15] D. Colton and R. Kress. *Inverse acoustic and electromagnetic scattering theory*, volume 93. Springer, 1998.

[16] S. Cools and W. Vanroose. Local Fourier Analysis of the Complex Shifted Laplacian preconditioner for Helmholtz problems. *Numerical Linear Algebra with Applications*, (submitted), 2012.

[17] H.C. Elman, O.G. Ernst, and D.P. O'Leary. A multigrid method enhanced by Krylov subspace iteration for discrete Helmholtz equations. *SIAM Journal on scientific computing*, 23(4):1291–1315, 2002.

[18] Y.A. Erlangga and R. Nabben. On a multilevel krylov method for the helmholtz equation preconditioned by shifted Laplacian. *Electronic Transactions on Numerical Analysis*, 31(403-424):3, 2008.

[19] Y.A. Erlangga and R. Nabben. Algebraic multilevel krylov methods. *SIAM Journal on Scientific Computing*, 31:3417–3437, 2009.

[20] Y.A. Erlangga, C.W. Oosterlee, and C. Vuik. On a class of preconditioners for solving the Helmholtz equation. *Applied Numerical Mathematics*, 50(3-4):409–425, 2004.

[21] Y.A. Erlangga, C.W. Oosterlee, and C. Vuik. A novel multigrid based preconditioner for heterogeneous Helmholtz problems. *SIAM Journal on Scientific Computing*, 27(4):1471–1492, 2006.

[22] Y.A. Erlangga, C. Vuik, and C.W. Oosterlee. Comparison of multigrid and incomplete LU shifted-Laplace preconditioners for the inhomogeneous Helmholtz equation. *Applied Numerical Mathematics*, 56(5):648–666, 2006.

[23] O.G. Ernst and M.J. Gander. Why it is difficult to solve Helmholtz problems with classical iterative methods. In *Numerical Analysis of Multiscale Problems. Durham LMS Symposium*. Citeseer, 2010.

[24] E. Haber and S. MacLachlan. A fast method for the solution of the Helmholtz equation. *Journal of Computational Physics*, 230(12):4403–4418, 2011.

[25] E. Hewitt and K. Stromberg. *Real and abstract analysis: a modern treatment of the theory of functions of a real variable*. 1975.

[26] D. Huybrechs and S. Vandewalle. On the evaluation of highly oscillatory integrals by analytic continuation. *SIAM Journal on Numerical Analysis*, 44(3):1026–1048, 2006.

[27] S.G. Johnson. Saddle-point integration of C$^\infty$ "bump" functions. *Manuscript. Available at http://math.mit.edu/∼stevenj/bump-saddle.pdf*, 2007.

[28] A. Laird and M. Giles. Preconditioned iterative solution of the 2d Helmholtz equation. Technical report, NA-02/12, Comp. Lab. Oxford University UK, 2002.

[29] C.W. McCurdy, T.N. Rescigno, and D. Byrum. Approach to electron-impact ionization that avoids the three-body coulomb asymptotic form. *Physical Review A*, 56(3):1958, 1997.

[30] K.O. Mead and L.M. Delves. On the convergence rate of generalized fourier expansions. *IMA Journal of Applied Mathematics*, 12(3):247–259, 1973.

[31] R.G. Newton. *Scattering theory of waves and particles*. Dover publications, 2002.

[32] D. Osei-Kuffuor and Y. Saad. Preconditioning Helmholtz linear systems. *Applied Numerical Mathematics*, 60(4):420–431, 2010.

[33] R.E. Plessix and W.A. Mulder. Separation-of-variables as a preconditioner for an iterative Helmholtz solver. *Applied Numerical Mathematics*, 44(3):385–400, 2003.

[34] B. Reps. *Iterative and multigrid methods for wave problems with complex-valued boundaries*. PhD thesis, Januari 2012, Universiteit Antwerpen, Belgium, 2012.

[35] B. Reps and W. Vanroose. Analyzing the wave number dependency of the convergence rate of a multigrid preconditioned Krylov method for the Helmholtz equation with an absorbing layer. *Numerical Linear Algebra with Applications*, 19(2):232–252, 2012.

[36] B. Reps, W. Vanroose, and H. bin Zubair. On the indefinite Helmholtz equation: Complex stretched absorbing boundary layers, iterative analysis, and preconditioning. *Journal of Computational Physics*, 229(22):8384–8405, 2010.

[37] B. Reps, W. Vanroose, and H. bin Zubair. Multigrid preconditioners based on polynomial smoothers for the Helmholtz equation with absorbing layers. *Submitted*, 2012.

[38] T.N. Rescigno, M. Baertschy, W.A. Isaacs, and C.W. McCurdy. Collisional breakup in a quantum system of three charged particles. *Science*, 286(5449):2474–2479, 1999.

[39] C.D. Riyanti, Y.A. Erlangga, R.E. Plessix, W.A. Mulder, C. Vuik, and C. Oosterlee. A new iterative solver for the time-harmonic wave equation. *Geophysics*, 71(5):E57–E63, 2006.

[40] A.H. Sheikh, D. Lahaye, and C. Vuik. A scalable Helmholtz solver combining the shifted Laplace preconditioner with multigrid deflation. Technical report, DIAM 11-01, Delft University of Technology, 2011.

[41] B. Simon. The definition of molecular resonance curves by the method of exterior complex scaling. *Physics Letters A*, 71(2):211–214, 1979.

[42] K. Stüben and U. Trottenberg. Multigrid methods: Fundamental algorithms, model problem analysis and applications. *Multigrid methods, Lecture Notes in Math.*, 960:1–176, 1982.

[43] U. Trottenberg, C.W. Oosterlee, and A. Schüller. *Multigrid*. Academic Press, New York, 2001.

[44] H.A. Van der Vorst. *Iterative Krylov methods for large linear systems*, volume 13. Cambridge University Press, 2003.

[45] H.A. van Gijzen, Y. Erlangga, and C. Vuik. Spectral analysis of the discrete Helmholtz operator preconditioned with a shifted Laplacian. *SIAM Journal on Scientific Computing*, 29(5):1942–1985, 2007.

[46] W. Vanroose, D.A. Horner, F. Martin, T.N. Rescigno, and C.W. McCurdy. Double photoionization of aligned molecular hydrogen. *Physical Review A*, 74(5):052702, 2006.

[47] W. Vanroose, F. Martin, T.N. Rescigno, and C.W. McCurdy. Complete photo-induced breakup of the H2 molecule as a probe of molecular electron correlation. *Science*, 310(5755):1787–1789, 2005.

[48] R.S. Varga. *Matrix iterative analysis*. Englewood Cliffs, N.J., Prentice-Hall, 2 edition, 1962.